International Journal of Pharmaceutics 702 (2026) 127203

Contents lists available at ScienceDirect

International Journal of Pharmaceutics

journal homepage: www.elsevier.com/locate/ijpharm

Repurposing glibenclamide for retinal protection: TUDCA-modified liposomes for ocular delivery

Sofia Dalla Lana [a], Francesco Bertocchi [b], Caterina Ricci [c], Cristina Sissa [b], Annalisa Bianchera [a], Elena Del Favero [c], Cristina Padula [a], Silvia Pescina [a], Patrizia Santi [a], Sara Nicoli [a,*]

[a] ADDRes Lab, Department of Food and Drug, University of Parma, Parco Area delle Scienze 27/a, 43124 Parma, Italy
[b] Department of Chemistry, Life Science and Enviromental Sustanainability, Univeristy of Parma, Parco Area delle Scienze 17/a, 43124 Parma, Italy
[c] Department of Medical Biotechnologies and Translational Medicine, LITA, University of Milan, 20054 Segrate, MI, Italy

ARTICLE INFO

Keywords:
Glibenclamide
Ocular drug delivery
Liposomes
Tauroursodeoxycholic acid (TUDCA)
Deformability
Neuroprotection

ABSTRACT

Glibenclamide, widely used as an oral treatment for type 2 diabetes, represents a promising example of drug repurposing. This second-generation sulfonylurea has demonstrated neuroprotective effects on ocular tissues following oral administration, showing potential benefits in the prevention and management of diabetic retinopathy and age-related macular degeneration (AMD). These findings suggest that local administration could be particularly advantageous for patients not receiving systemic glibenclamide therapy. However, to enhance ocular bioavailability and achieve sustained drug release, an appropriate delivery system is required. This study aimed to develop a topical liposomal formulation for the ocular delivery of glibenclamide. To improve penetration across biological barriers, liposome properties were optimized by incorporating tauroursodeoxycholic acid (TUDCA), a bile salt derivative that also demonstrated neuroprotective activity. The inclusion of this molecule within the lipid bilayer impacted phospholipid organization, increasing vesicle deformability, as confirmed by small-angle X-ray scattering (SAXS) analysis. Glibenclamide loading did not affect vesicle deformability and was higher in TUDCA-modified liposomes compared to conventional liposomes. *Ex vivo* permeation studies using isolated porcine ocular tissues (cornea, conjunctiva, and sclera) further supported TUDCA's role as an edge activator, enhancing drug penetration. Notably, glibenclamide liposomes were also able to accumulate in the sclera, forming a reservoir for sustained release over time. Finally, the liposomal formulation demonstrated good tolerability in ARPE-19 cell lines, highlighting its potential as a safe and effective system for ocular delivery of glibenclamide.

1. Introduction

Approximately 588.7 million people worldwide between 20 and 79 years have diabetes. The incidence is expected to further increase rapidly, reaching 852.5 million in 2050 (Diabetes Atlas, 2025). Diabetic retinopathy (DR) is one of the main causes of blindness and visual impairment related to diabetes, with an incidence of 146 million adults in the world (Teo et al., 2021; World Health Organization, 2019). However, non-painful and non-invasive treatments to reduce or prevent retinal degeneration are not currently approved (Appell et al., 2024). Regular eye exams, blood sugar, and blood pressure control are the only way to prevent or reduce the adverse effects of diabetes on the ocular tissues (Chong et al., 2024). Focusing on the prevention of the ocular complication, topical formulations like eye drops could be a valid support, since they are easy to use for patients and low-cost (Li et al., 2019).

In recent years, drug repositioning has gained significant traction thanks to the use of well-known molecules with new indications, avoiding new research and new clinical trials (Jourdan et al., 2020). Among these, glibenclamide (Fig. 1) is a second-generation sulfonylurea commonly used in oral therapy to manage type 2 diabetes in adults, which has also demonstrated neuroprotective properties. In fact, it exerts neuroprotective activity in the retina against oxidative stress, cell

* Corresponding author.
E-mail addresses: sofia.dallalana@unipr.it (S. Dalla Lana), francesco.bertocchi@unipr.it (F. Bertocchi), caterina.ricci@unimi.it (C. Ricci), cristina.sissa@unipr.it (C. Sissa), annalisa.bianchera@unipr.it (A. Bianchera), elena.delfavero@unimi.it (E. Del Favero), cristina.padula@unipr.it (C. Padula), silvia.pescina@unipr.it (S. Pescina), patrizia.santi@unipr.it (P. Santi), sara.nicoli@unipr.it (S. Nicoli).

https://doi.org/10.1016/j.ijpharm.2026.127203
Received 3 June 2026; Received in revised form 15 July 2026; Accepted 16 July 2026
Available online 24 July 2026
0378-5173/© 2026 The Author(s). Published by Elsevier B.V. This is an open access article under the CC BY license (http://creativecommons.org/licenses/by/4.0/).

death, and inflammation, improving retinal function in diabetic rodent models via SUR1 binding (Berdugo et al., 2021; Picard et al., 2024). Importantly, the neuroprotective activity of glibenclamide occurs at doses significantly lower than those required for glycemic control, opening the door to its use via topical ocular administration (e.g., eye drops) with minimal risk of systemic side effects. This approach is particularly relevant for patients who are not already receiving oral glibenclamide, allowing its repositioning specifically for ocular complications such as diabetic retinopathy and age-related macular degeneration (AMD). Indeed, a retrospective case-control study found that glibenclamide use in diabetic patients was associated with a reduced risk of new-onset dry AMD (Picard et al., 2024).

Despite their ease of administration and patient compliance, eye drops are generally ineffective at delivering drugs to the posterior segment of the eye due to the presence of multiple anatomical and physiological barriers, as well as rapid clearance mechanisms (Gabai et al., 2023; Yang and Lockwood, 2022). To overcome these limitations, nanocarrier-based systems such as liposomes, in addition to offering biocompatibility, provide sustained drug release and can enhance tissue penetration (Li et al., 2019; Kumar and Tiwari, 2025; López-Cano et al., 2021). In principle, the ability of liposomes to reach deeper ocular tissues may be enhanced by increasing their deformability. Deformable liposomes—also referred to as elastic or ultra-flexible vesicles—have shown improved penetration across biological barriers, particularly in the context of transdermal delivery (Park and Kim, 2023), where a clear correlation between vesicle flexibility and skin permeation has been established (Schlich et al., 2022). This enhanced deformability is typically achieved through the incorporation of edge activators, surfactant-like molecules that fluidize the lipid bilayer, allowing vesicles to adapt their shape without compromising structural integrity (Kumar and Tiwari, 2025; Trivedi et al., 2021; Zhao and Mao, 2021). While similar direct evidence is still limited in the ocular field, it is reasonable to expect that increased vesicle deformability could also facilitate penetration across ocular barriers.

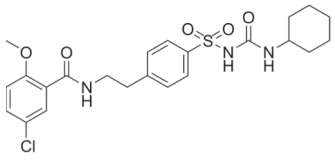
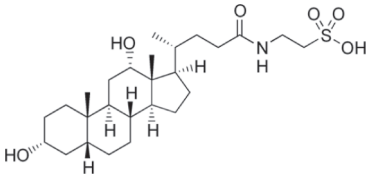
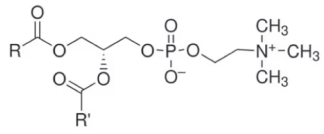
In this context, tauroursodeoxycholic acid (TUDCA) (Fig. 1), a hydrophilic secondary bile acid derived from microbial metabolism of primary bile acids, emerges as a particularly interesting excipient. Thanks to its amphiphilic structure and surface-active properties, TUDCA can act as an edge activator, potentially improving liposome deformability. In addition to its technological role, TUDCA also exhibits pleiotropic biological effects, including antioxidant, antiapoptotic, and anti-inflammatory activity (Fu et al., 2021). Although its precise mechanism of action is not yet fully elucidated, TUDCA has demonstrated significant neuroprotective potential in various models of neurodegeneration and disease, including diabetic retinopathy (Daruich et al., 2022; Daruich et al., 2019; Khalaf et al., 2022; Li et al., 2024).

This work aims to develop a topical liposomal formulation for the ocular delivery of glibenclamide, incorporating TUDCA, which plays a dual role: as a neuroprotective agent and as a functional excipient that enhances the technological performance of the delivery system.

2. Materials and methods

2.1. Materials

Glibenclamide (MW 494 g/mol; LogP: 3.75; melting point

Compound	Physicochemical Properties	Molecular Structure
Glibenclamide	**MW** (g/mol): 494 **Log P:** 3.75 **pKa**: 5.3	
TUDCA Tauroursodeoxycholic acid	**MW** (g/mol): 499.7	
Lipoid S75: Phosphatidylcholine n.l.t. 70.0 Phosphatidic acid n.m.t. 3.0 Phosphatidylinositol n.m.t. 1.5	**MW** (g/mol): 756.1 711.77 867.1	Phosphatidylcholine  R, R' = fatty acid residues R, R'=fatty acid residues: Linoleic (58-65%); palmitic (12-17%); oleic (8-12%); linolenic (5-9%); stearic (2-5%)

n.l.t. = not less than; n.m.t. = not more than.

Fig. 1. Drug and excipients used for liposomes preparation with their main chemical features and molecular structure.

169–170 °C) was purchased from ThermoFisher (Kandel) GmbH (Germany). Lipoid S75 (composition in Fig. 1) was a kind gift from Lipoid GmbH (Ludwigshafen, Germany). Tauroursodeoxycholic acid (TUDCA) Sodium Salt (MW 521.7 g/mol) was purchased from EMD Millipore Corp, USA. 2-hydroxypropyl-β-cyclodextrin (KLEPTOSE® HPB oral grade, HPβCD) was a gift from Roquette (Lestrem, France). Acetonitrile and ethanol 96 % were of HPLC grade. Nile Red was acquired from Sigma-Aldrich (Missouri, USA). 1,10-dioctadecyl-3,3,30,30-tetramethyl- indodicarbocyanine perchlorate (DiD), and 1,6-diphenyl-1,3,5-hexatriene (DPH) were purchased from ThermoFisher (Invitrogen). Phosphate buffer saline (PBS) was prepared by adding 8.80 g/L of NaCl, 2.37 g/L of Na_2HPO_4, and 0.19 g/L of KH_2PO_4 to purified water. Then, H_3PO_4 was used to decrease the pH value to 7.4. NaCl 0.9 % w/v was prepared by dissolving 9 g of NaCl in 1L of purified water.

2.2. Glibenclamide quantification method

The analytical method was validated using an HPLC-UV system (1260 Infinity II, Agilent Technologies, Santa Clara, CA, USA) in isocratic conditions. A Luna® C_8 50 x 3 mm, 3 μm (Phenomenex) column thermostated at 30 °C was used. The mobile phase, pumped at 0.6 mL/min, was composed of 0.3 % v/v acetic acid and CH_3CN in a 53:47 (v/v) ratio. The retention time of glibenclamide, quantified by UV absorbance at 230 nm, was 3.1 min. The injection volume was 20 μL. Two calibration curves were built in the intervals 0.05–1 μg/mL and 1–25 μg/mL. Standard solutions were prepared using a 50:50 (v/v) MeOH:H_2O mixture.

2.3. Drug solubility studies

To measure the solubility of glibenclamide, an excess amount of drug was added to purified water, PBS pH 7.4, NaCl 0.9 %, ethanol, and a solution of 12.3 mg/mL 2-hydroxypropyl-β-cyclodextrin (HPβCD) in PBS. After stirring for 72 h at 37 °C, samples were centrifuged at 12,000 rpm for 15 min. The supernatants were collected, diluted, and analyzed by HPLC-UV.

2.4. Preparation of liposomes

Liposomes were prepared by the ethanol injection method. Lipoid S75, a pharmaceutical-grade soybean phospholipid mixture (Fig. 1) widely used in pharmaceutical liposomal formulations, was dissolved in ethanol at 100 mg/mL, and 300 μL of this solution were injected into 4 mL of the aqueous phase (PBS pH 7.4), stirred at 1000 rpm. Edge activator, TUDCA, was dissolved in the ethanol solution with Lipoid S75 (Lipoid S75:TUDCA ratio: 2.5:1 by weight). After the injection, the formulations were kept under stirring overnight at room temperature to allow ethanol evaporation. Glibenclamide-loaded liposomes were prepared with the same procedure, by dissolving the drug at saturation in the ethanolic phase (glibenclamide solubility in ethanol was determined and resulted in 2.05 ± 0.42 mg/mL) before Lipoid S75 and TUDCA addition. To increase loading reproducibility, both the ethanol and water phases were thermostated at 37 °C. After ethanol evaporation, liposomes were centrifuged (10 min at 3000 rpm) to remove the non-encapsulated drug. To quantify the amount of glibenclamide encapsulated, liposomes were first diluted 1:100 with methanol followed by a further 1:1 dilution with purified water. The solution was analyzed by HPLC. To evaluate the effective loading of GLI in the liposomes, centrifugal filters (cutoff: 30 kDa) were used. The concentration of glibenclamide in the filtrate (non-encapsulated drug) resulted approximately equal to the solubility in PBS. A further test was performed to evaluate the possible solubilizing role of the residual ethanol used during the preparation: mock liposomes (i.e. same procedure but without Lipoid S75 and TUDCA) were prepared, and the GLI solubility obtained was comparable to that in PBS only (12.15 ± 0.34 μg/mL).

Fluorescent probes –loaded liposomes were also prepared. The probes, either 5 x 10^{-5} M and 10^{-6} M Nile Red, 10^{-6} M and 10^{-7} M DiD (1,10dioctadecyl-3,3,30,30-tetramethylindodicarbocyanine perchlorate), and 2 x 10^{-6} M DPH (1,6-diphenyl-1,3,5-hexatriene) (concentrations in the final formulations) were dissolved in the ethanolic phase.

2.5. Liposomes characterization: dynamic light scattering analysis

Liposomes were characterized in terms of size, zeta potential, and pH. Size and Z-potential data were collected using a Zetasizer Malvern (Ver. 7.12, Malvern Instruments LTD, Malvern, Worcestershire, UK). To obtain size data, samples were diluted with PBS and analyzed at 25 °C with an incidence angle of 173°. For zeta potential analysis, the samples were diluted 1:10 with KCl 2 mM solution.

2.6. SAXS analysis

Small-angle X-ray scattering (SAXS) measurements were performed at the European Synchrotron Radiation Facility (ESRF) in Grenoble, France, using beamline BM29b (Del Favero et al., 2024). Scattering curves were collected as a function of the momentum transfer $q = \frac{4\pi}{\lambda}\sin\left(\frac{\theta}{2}\right)$, where θ is the scattering angle and λ is the X-ray wavelength of the incident beam. Raw data were processed using the standard pipeline provided at BM29, including background subtraction, normalization to transmitted beam intensity, and calibration of the q-scale. The resulting profiles were used to extract information on particle size, morphology, and internal organization in solution. Scattering curves were analyzed using SasView version 5.0.6 (M. Doucet et al. SasView Version 5.0.6, https://doi.org/10.5281/zenodo.7581379), applying the Lamellar_Caille_HG model for samples displaying lamellar order. This model describes the scattering from a stack of bilayers with finite positional correlations and incorporates both the bilayer form factor (head–group + tail representation) and the Caillé paracrystalline structure factor. SAXS intensity profile represents the electron density distribution within the particle. The liposome is modelled as a hollow particle with a shell composed by a stack of lipid bilayers. Each lipid bilayer is modelled with three layers, each one with given electron density and thickness in agreement with the expected head–tail-head structure of lipid bilayers. The values of the electron densities in the head or tail layers are the average values among all the components present in that layer.

2.7. Deformability test and flexibility calculation

The deformability test was adapted from the method proposed by Park et al (Park and Kim, 2023). Unlike the original procedure, a constant force was applied, and the time required for the extrusion of the formulation was recorded. Particularly, a 1 kg weight was put on the plunger of a Hamilton syringe connected with an extruder system. The time needed to perform the extrusion through a 50 nm pore size was measured, and the extrusion rate was calculated. The test was carried out maintaining the extruder system at 65 °C, above the transition temperature of Lipoid (45 °C (Badran et al., 2012). The procedure has been detailed in the Supplementary Material section, Fig. 1S. The experiment was performed for all formulations previously described. In addition, controls were also tested, where edge activator (TUDCA) was added at the same concentration, to preformed Lipoid S75 vesicles. Flexibility of vesicles was calculated using the following equation:

$$Flexibility\left(mg/s\right) = R\,x\left(r_v/r_p\right)^2 \quad (1)$$

where R (mg/s) was calculated from the extrusion rate (μL/s) taking into consideration the concentration of lipid (or lipid + TUDCA) of each formulation, r_v was the size of vesicles after the first cycle of extrusion

measured by DLS, and r_p was the pore size of the membrane (50 nm) (Park and Kim, 2023).

2.8. Extrusion of liposomes

Liposome suspensions were extruded using the Avanti Mini-Extruder (Avanti Research, Alabama, USA). Samples were thermostated for 5 min at 65 °C in the extruder apparatus and then extruded six times at the same temperature through a 50 nm pore size polycarbonate membrane. Liposomes were then analyzed by DLS to verify the reduction of the size and PdI after each cycle.

2.9. Determination of encapsulation efficiency and drug loading

The encapsulation efficiency and the drug loading were calculated as follows:

$$\%\,Drug\,Loading = \frac{Q_{GLI}}{Q_L + Q_{GLI}}\,x\,100 \quad (2)$$

$$\%\,Encapsulation\,Efficiency = \frac{Q_{GLI}}{Q_T}\,x\,100 \quad (3)$$

where Q_L was the amount of excipients (i.e. Lipoid S75 or Lipoid S75 + TUDCA) in the liposomal formulation, Q_{GLI} was the amount of glibenclamide loaded, quantified by HPLC-UV and Q_T was the amount of glibenclamide used to prepare liposomes.

2.10. Permeation across porcine ocular tissues

2.10.1. Isolation of cornea, conjunctiva and sclera

Porcine eyeballs were obtained from a local abattoir (Macello Annoni S.p.A., Parma, Italy). After enucleation, the eyes were stored in a saline solution at 4 °C until the dissection. Cornea, conjunctiva and sclera were isolated following the methodology reported in other studies (Pescina et al., 2019); (Pescina et al., 2020); (Pescina et al., 2012). Isolated corneas were obtained by cutting circumferentially beyond the limbus and mounted with the epithelial side in contact with the donor (Pescina et al., 2020). The conjunctiva was mounted carefully on the receptor compartment, still attached to the eyeball. After assembling the cell, the eye bulb was removed by cutting away the excess conjunctiva (Pescina et al., 2019). Instead, to obtain isolated sclera and choroid, the anterior segment was removed. The eye bulb was emptied of the vitreous body and cleaned of the retinal pigmented epithelium (RPE) and retina. By cutting along the ciliary arteries, half of the sclera (with/without optic nerve) was obtained (Pescina et al., 2012). Conjunctiva and cornea were used within 3–4 h from the animal sacrifice.

2.10.2. Permeation and retention studies

Permeation studies were performed using Franz-type diffusion cells (DISA, Milano, Italy) with a permeation area of 0.6 cm^2 for transscleral studies, and 0.2 cm^2 in the case of conjunctiva and cornea. The receptor chamber contained approximately 4 mL of degassed 12.3 mg/mL HPβCD solution in PBS (drug solubility: *approx.* 100 μg/mL, Table 1), thermostated at 37 °C, and kept under magnetic stirring. The donor chamber was filled with 300 μL of liposomal formulation and then covered with parafilm. The receptor fluid was sampled at predetermined time points and analyzed by HPLC-UV. The flux J (μg/cm^2 h) was obtained from the slope of the regression line at the steady state.

In the case of the cornea, the drug content inside the tissue at the end of the experiment was also evaluated: the donor was removed, the cornea was rinsed with saline solution three times and 0.5 mL of a MeOH:H_2O 80:20 (v/v) mixture were added. The samples were sonicated for 10 min, extracted overnight at room temperature, then centrifuged at 12000 rpm for 10 min. The supernatant was analyzed by HPLC-UV. The extraction procedure was validated, and the recovery percentage was around 90 % (see Supplementary Materials for details, Table 1S).

Table 1
Glibenclamide Solubility data.

Solvent	GLI Concentration (μg/mL) ± SD
Water	6.40 ± 3.21
Phosphate buffer	8.93 ± 2.00
NaCl 0.9 %	3.95 ± 2.71
Ethanol	2048.54 ± 418.05
HPβCD (12.3 mg/mL)	100.05 ± 7.18

2.11. Two-photon microscopy

Permeation experiments across isolated cornea (application time 2 h), conjunctiva (application time 2 h), and sclera (application time 1 h) were performed with DiD-loaded liposomes (see par. 2.4) following the protocol described in paragraph 2.10. Porcine ocular samples were then analyzed with a Two-Photon Microscope Nikon A1R MP + Upright equipped with a femtosecond pulsed laser Coherent Chameleon Discovery (~ 100 fs pulse duration with 80 MHz repetition rate, tunable excitation range 660–1320 nm). A 25 × water dipping objective with numerical aperture 1.1 and 2-mm working distance was employed for focusing the excitation beam and for collecting the two-photon excited fluorescence (TPEF) and the second harmonic generation (SHG) signals. TPEF/SHG signal was directed by a dichroic mirror to a series of two non-descanned detectors (high-sensitivity GaAsP photomultiplier tubes), allowing fast image acquisition. The two detectors are preceded by optical filters allowing the simultaneous acquisition of two separated channels: green channel (506–593 nm) and red channel (604–679 nm). Imaging overlay of the two channels and processing was performed by the operation software of the microscope. For all studied samples, laser power was held at 10 %, excitation wavelength was 1150 nm, and detector gains were 35 (green channel) and 100 (red channel). The excitation wavelength was chosen to observe the SHG signal of collagen in the green channel, and at the same time to effectively excite the DiD dye, whose emission signal can be collected in the red channel. For each sample, Z-stacks were performed on a 0.5x0.5 mm area from the surface to a depth of ca. 120 μm. Images at varying depths were also taken, sometimes with zooms on specific areas.

2.12. Freeze-drying

Vesicles were freeze-dried using the Laboratory freeze dryer Alpha 2–4 LSCplus (Martin Christ, Osterode am Harz, Germany). Different excipients were examined as cryoprotective agents following literature (Franzé et al., 2018). Glucose and mannitol at 7.5 % w/w, sucrose and lactose at 15 % w/w were added into the aqueous phase after the evaporation of ethanol. In further tests, lactose was also added in two steps, to reach a concentration of 5 % w/w before the ethanol injection into the aqueous phase, and a further concentration of 15 % w/w afterward. Freeze-dryer program was adapted from Sebaaly et al. (Sebaaly et al., 2016). Liposomal suspensions (2 mL) were frozen at −80 °C in a glass vial and then transferred to the freeze-dryer pre-cooled at –40 °C. After equilibration (5 min at –40 °C), primary drying was performed at 0.15 mbar and –40 °C for 40 min, followed by a gradual increase in 5 h to –38 °C, keeping constant for 30 min. Then, in 30 min –10 °C and 0.10 mbar were reached and maintained for 3 h. In 30 min, secondary drying proceeded at 0.015 mbar for 6 h at 5 °C and, in 10 min, 10 °C was reached and maintained for 9 h. In 20 min, the temperature reached 20 °C and the pressure of 0.010 mbar was maintained for 10 h. The vials were collected, closed, and stored at 4 °C. The liposomes were reconstructed with PBS to their original volume (2 mL) before characterization using consecutive cycles of vortexing. Samples were analyzed by DLS to verify the size and polydispersity index of vesicles, and by HPLC-UV to quantify the amount of glibenclamide loaded.

2.13. Cell viability assay

The colorimetric 3-(4,5)dimethylthiazol-2-yl)-2,5-diphenyltetrazolium bromide (MTT) assay was used to measure cell viability. The ARPE-19 cell line, retinal pigment epithelial (RPE) cell line, was acquired by ATCC (Virginia, USA), grown to 90 % confluence in DMEM/F12 + 10 % FBS with penicillin and streptomycin (culture medium), and kept in an incubator with 5 % CO_2. The cells were collected from cell plates by the addition of trypsin-EDTA and seeded at a density of 9,000 cells/well in 96-well plates and grown in culture medium for 48 h. The medium was removed, and the cells were treated with 100 μL of different formulations for 4 h at 37 °C. Particularly, TUDCA solutions (6 mM stock solution prepared in NaCl 0.9 %), liposomes with/without TUDCA, and GLI-loaded liposomes with/without TUDCA were tested at different concentrations (see Fig. 10) after dilution in Hank's balanced salt solution (HBSS). To verify cell toxicity, 20 % v/v solution of ethanol in HBSS was used as a positive control, while HBSS was applied as an untreated negative control. After the incubation, liposomes were removed and 100 μL of MTT in HBSS 0.5 mg/mL were added to each well for 3 h. At the end of the treatment period, 100 μL of DMSO were added to dissolve the formazan crystals produced. A plate reader (SPARK10M, Tecan, Tecan Austria GmbH, Austria) was used to analyse the resulting solutions at 570 nm. Cell viability was obtained in percentage as follows, after subtraction of blank signal:

$$\text{Cell viability}\,(\%) = \frac{Abs\ sample\ \text{x}\ 100}{Abs\ control} \quad (4)$$

where the absorbance of the untreated control group corresponded to 100 % viability.

2.14. Statistical analysis

The data presented in this work are reported as average ± standard deviation (SD). The *t*-test was used to explore statistical significance, considering statistically different when $p < 0.05$. For the sake of clarity, in case of permeation across the conjunctiva, data in Fig. 3 are reported as average ± sem (standard error of the mean), as indicated in the figure legend together with the indication of the replicate number.

3. Results and discussion

3.1. Glibenclamide solubility

Solubility data are reported in Table 1. As expected, the solubility of the drug in water, phosphate buffer, and NaCl 0.9 % was very low, confirming literature data (Maharjan et al., 2022). To increase the solubility and maintain sink conditions in permeation experiments, HPβCD can be added to the receptor solution. Solubility in ethanol, used for liposomes preparation, was around 2 mg/mL.

3.2. Characterization of liposomes

The first part of the work was related to the optimization and characterization of blank and loaded liposomes, highlighting size, PdI, zeta potential, and flexibility of formulations made with/without TUDCA.

3.2.1. Dynamic light scattering: size and zeta potential

The values for blank and TUDCA-loaded liposomes are reported in Table 2. Vesicles made with Lipoid S75 were slightly bigger than liposomes made with the edge activator. The value of the polydispersity index was below 0.2 for all formulations. The zeta potential was approximately − 30 mV for Lipoid S75 liposomes, reflecting the presence of minor amounts of anionic phospholipids (e.g., phosphatidic acid and phosphatidylinositol) in the soybean lecithin mixture, while the incorporation of the negatively charged TUDCA further decreased the zeta potential to approximately − 38 mV.

Table 2
Characteristics of blank liposomes with/without TUDCA.

	Size ± SD (nm)	PdI ± SD	Z-potential ± SD (mV)
Lipoid S75	152.5 ± 4.4	0.17 ± 0.01	−30.7 ± 3.2
Lipoid S75 + TUDCA	132.8 ± 12.0	0.15 ± 0.02	−38.1 ± 3.8

3.2.2. SAXS analysis

Small-angle X-ray scattering (SAXS) was employed to probe the nanoscale organization of Lipoid-based structures and to assess how their architecture is modified upon incorporation of TUDCA. The measured scattering profiles (Fig. 2) gave structural information on the nm length-scale, corresponding to the internal arrangement of the lipid particles. The SAXS profiles of Lipoid S75 (blue dots) and phosphatidylcholine with tauroursodeoxycholic acid (red dots, Lipoid S75-TUDCA) showed clear structural differences. In the mid-q region, Lipoid S75 exhibited a peak at $q \approx 1\ nm^{-1}$, corresponding to a periodic distance of ~ 6.3 nm (Table 3), indicating a multi-lamellar internal organization. Conversely, Lipoid S75-TUDCA displayed a broader peak at $q \approx 0.79\ nm^{-1}$, corresponding to a higher interlamellar periodic distance ($d \approx 8.0$ nm) with expanded bilayers or thicker water layers between adjacent lamellae. These differences suggested the presence of TUDCA into lipid-based particles.

A detailed description of the internal arrangement is obtained by modelling the intensity profile using a lamellar-Caillé model, where the periodic bilayer stacking and its thermal fluctuations are described through a structure factor that includes a fluctuation parameter (the Caillé parameter) quantifying the degree of lamellar disorder (Fig. 2, black lines). The model of Lipoid particle with the lamellar Caillé-type model revealed a well-defined multilamellar organization, characterized by a d-spacing of 6.3 nm, coherent stacking over several bilayers ($N = 6$), and a moderate Caillé parameter indicative of limited membrane fluctuations. The phospholipid bilayers showed a thickness of 4.97 nm and were separated by 1.3 nm of interlamellar hydration layers.

Upon addition of TUDCA, the SAXS pattern showed marked changes: the optimal model required fewer coherently stacked lamellae ($N = 3$), the d-spacing increased to 8.48 nm, and the Caillé parameter rose slightly, indicating enhanced disorder and reduced long-range lamellar correlation.

Notably, the fitted SLD values (Table 3) showed a decrease in the tail-region SLD and a slight increase in the head-region SLD, while the geometric thicknesses of both head and tail remained comparable to those of the pure Lipoid system. This combination of features pointed to TUDCA localizing predominantly at the headgroup-water interface and within the interlamellar space, where it perturbs packing, increases hydration, and disrupts stacking coherence without penetrating deeply into the hydrophobic layer. Overall, the SAXS-derived parameters outlined that TUDCA acts as a surface disruptor that loosens heads and tails packing, enlarges water spacing, and destabilizes multilamellar order while preserving bilayer integrity.

3.2.3. Deformability test and flexibility calculation

Extrusion rate through a 50 nm pore polycarbonate filter was used to evaluate liposome deformability (Guillot et al., 2023); (González-Rodríguez et al., 2016). This pore size was intentionally selected to improve the discrimination between formulations. Since liposome populations exhibited mean diameters slightly above 100 nm, the use of a 50 nm membrane imposed a more stringent deformation requirement than a 100 nm membrane, thereby enhancing the sensitivity of the test to differences in membrane flexibility. Fig. 3 illustrates the extrusion rate of blank and GLI-loaded liposomes.

This preliminary assay demonstrates that the composition of vesicles affects their flexibility. Indeed, a very low extrusion rate was observed for liposomes prepared with Lipoid S75 only (0.37 ± 0.14 μL/s) while

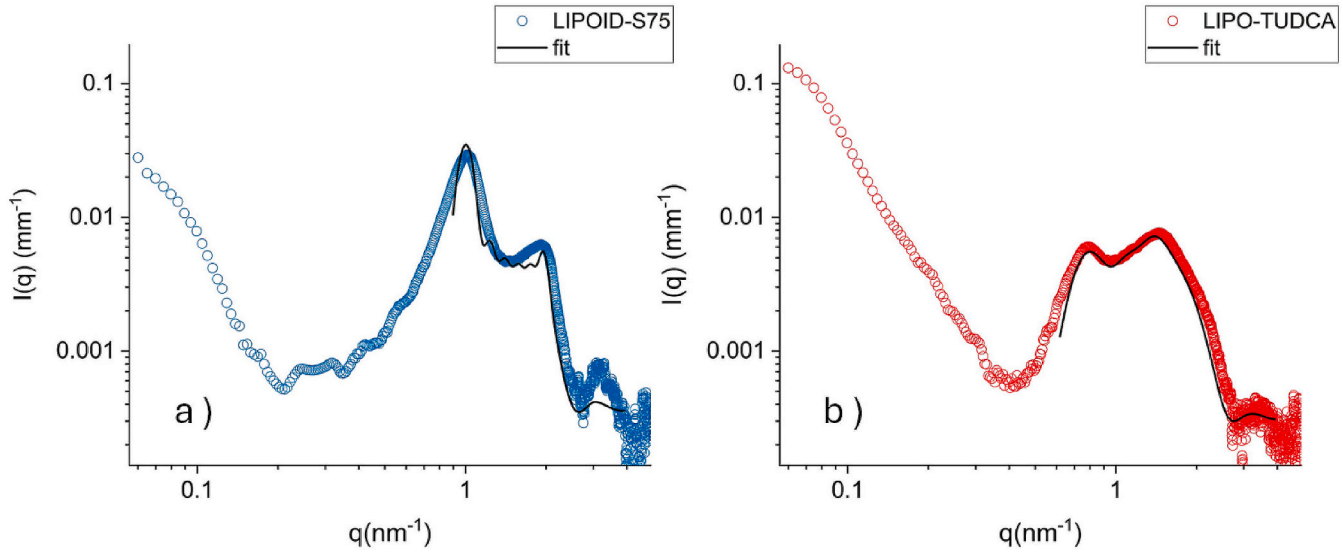


Fig. 2. SAXS spectra (Intensity versus scattering vector q) of LIPOID S75 (left panel) and LIPOID S75 + TUDCA (right panel). In both panels the fitted data are reported in black solid line.

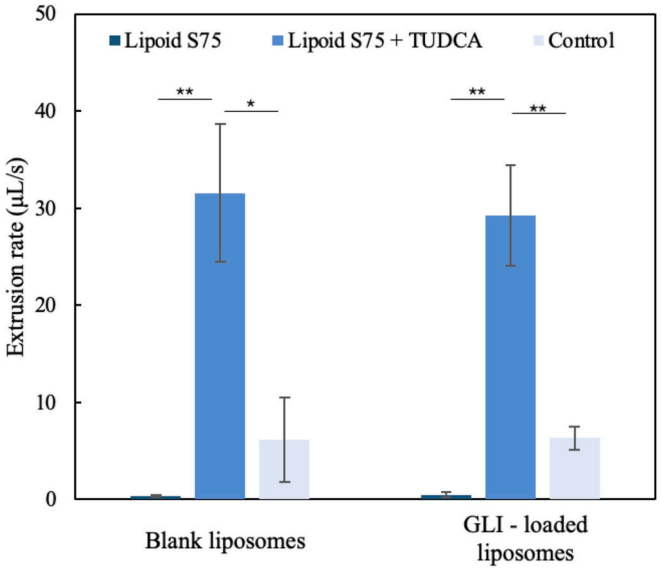


Fig. 3. Extrusion rate of liposomes obtained with a preliminary deformability test. Control samples are represented by Lipoid S75 liposomes with the addition of TUDCA after vesicles' formation.

the presence of edge activator (TUDCA) increased the value to 31.59 ± 7.09 µL/s. The extrusion rate found in control tests (i.e. TUDCA added after Lipoid S75 vesicles' formation) was higher than that of vesicles prepared with Lipoid S75 only, due to the lubricating effect of TUDCA, having surfactant properties. However, this value was significantly lower than that of liposomes prepared with TUDCA, confirming the incorporation of the edge activator within the bilayer, as also described by SAXS spectra. This observation is consistent with the behavior of deformable liposomes, which are characterized by the ability to pass through pores smaller than their diameter with reduced resistance, owing to increased membrane elasticity (Kumar and Tiwari, 2025; Mosallam et al., 2021; Singh et al., 2017).

Despite the clear difference in the extrusion rate, the liposome size after extrusion was comparable between Lipoid S75 liposomes and those containing TUDCA, being approx. 80 nm in both cases (Fig. 2S). A similar behavior is, however, also shown by a well-known edge activator, i.e. tween 80, as illustrated in Supplementary material (Fig. 2S). This could be explained by the hydrophilicity of TUDCA, which, contrary to what happens to more lipophilic bile salts such as cholate (Sharma et al., 2010), does not penetrate deeply into the membrane bilayer. Indeed, molecular dynamic simulation tests performed on POPC (1-palmitoyl–2–oleoyl–sn–glycerol–3–phosphocholine) membranes suggest an alignment parallel to the surface, with their sulfate groups directed toward the aqueous phase, adsorbing at the lipid/water interface. Such a TUDCA arrangement may explain the limited (although noticeable) changes in the polarity and fluidity of the investigated model membranes (Sabat et al., 2021). This observation is also in agreement with SAXS data, highlighting that TUDCA localizes predominantly at the headgroup-water interface and within the interlamellar space, where it perturbs packing, increases hydration, and disrupts stacking coherence without penetrating deeply into the hydrophobic layer.

Data reported in Fig. 3 also demonstrate that the encapsulation of glibenclamide within the vesicles did not significantly increase the stiffness of liposomes. From the data presented in Fig. 3, the flexibility (mg/s) was calculated using Eq. (1) (Park and Kim, 2023) (Table 2S). Comparing conventional liposomes (i.e. prepared with Lipoid S75 only), the presence of TUDCA increased the flexibility value for both blank (1.02 ± 0.23 mg/s), and drug-loaded liposomes (0.85 ± 0.18 mg/s). All flexibility data are shown in Supplementary Materials, Table 2S.

3.3. Glibenclamide-loaded liposomes

3.3.1. Glibenclamide loading

The amount of glibenclamide encapsulated within vesicles was evaluated by HPLC-UV (Table 4). Glibenclamide was successfully encapsulated in all formulations, increasing the solubility at least 10 times compared to its value in aqueous solutions. Particularly, the higher percentage of entrapment efficiency was for liposomes prepared with TUDCA. Given its lipophilicity (LogP: 3.754), glibenclamide is probably loaded inside the lipidic double layer, however, its presence did not impact vesicle flexibility; size and zeta potential remained unchanged as well.

To investigate the effect of vesicle size on permeation through tissues, GLI-loaded extruded liposomes (6 cycles) were also prepared. Table 5 shows the impact of the extrusion cycles on size and polydispersity index, which decreased well below 0.1. The amount of glibenclamide encapsulated within the vesicles was not affected by the

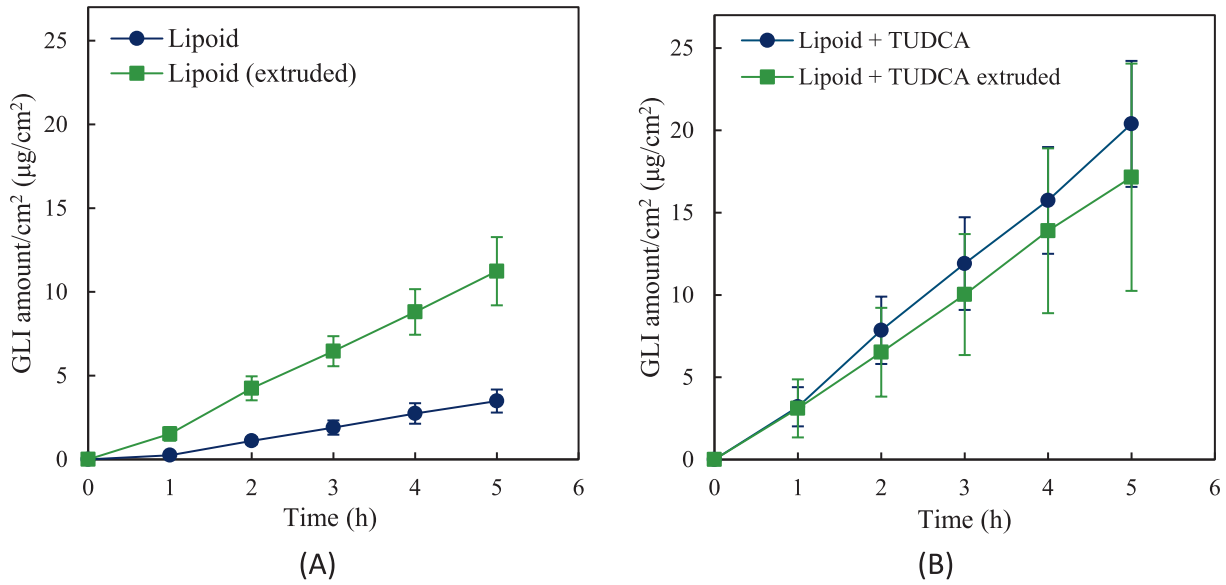


Fig. 4. Permeation of glibenclamide across the conjunctiva from liposomes made of Lipoid S75 only (Panel A) and made of Lipoid S75 and TUDCA (Panel B). Average ± sem (n > 4).

Table 3
Structural parameters of blank liposomes with/without TUDCA.

	Lipoid S75	Lipoid S75 + TUDCA
Tail length (nm)	10	10
Head length (nm)	16.6	16
D spacing (nm)	6.3	8.48
Tail SLD (10–6 Å-2)	7.5	6.76
Head SLD (10–6 Å-2)	11.7	12
Number of coherent layers	6	3

extrusion process.

3.4. Ex vivo permeation studies

To reach the posterior segment of the eye, the drug can follow the conjunctival–scleral route or the corneal pathway (Varela-Fernández et al., 2020; Qi et al., 2023). Based on this rationale, we evaluated the tissue permeation of GLI in liposomal formulations across cornea, conjunctiva and sclera. Although it remains unclear whether liposomes administered topically penetrate intact to the sclera or sclera/choroid interface, these *ex vivo* data are useful for formulation characterization and may also be relevant for alternative administration routes such as periocular delivery.

3.4.1. Conjunctiva

Both non-extruded (larger, native size) and extruded (smaller) vesicles were tested to explore the influence of vesicle size and flexibility on tissue permeation. The results revealed that, in conventional liposomes, extrusion significantly enhanced tissue penetration, indicating that a smaller size improves permeation when deformability is limited. In contrast, for TUDCA-modified liposomes, no significant difference was observed between extruded and non-extruded samples, suggesting that increased flexibility can compensate for a larger size. Flux (J) values showed a statistically significant difference ($p < 0.05$) between extruded (2.63 ± 1.03 µg/cm^{2}h) and non-extruded (0.80 ± 0.41 µg/cm^{2}h) liposomes composed solely of Lipoid S75, while no such difference between extruded and non-extruded was observed in formulations containing TUDCA (4.15 ± 0.90 vs 2.91 ± 0.66 µg/cm^{2}h).

3.4.2. Sclera

A similar result was observed across isolated porcine sclera (Fig. 5), indicating that the effect of liposome deformability extended to both epithelial tissues and collagen-rich connective tissues. This finding is somewhat unexpected, as the underlying permeation mechanisms in these two tissues are likely different: in the sclera, drug transport primarily occurs through diffusion within hydrophilic pores of the collagen matrix, whereas, in the conjunctiva, it may involve interactions with epithelial cells and intercellular junctions (Varela-Fernández et al., 2020).

In this case as well, flux values showed a statistically significant difference ($p < 0.05$) between extruded (0.60 ± 0.09 µg/cm^{2}h) and non-extruded (0.33 ± 0.09 µg/cm^{2}h) liposomes composed solely of Lipoid S75. In contrast, liposomes with TUDCA exhibited no such difference (extruded: 0.84 ± 0.15 µg/cm^{2}h, non-extruded: 0.87 ± 0.17 µg/cm^{2}h). Within this matrix, larger deformable liposomes may continuously adapt

Table 5
Characteristics of glibenclamide-loaded liposomes after 6 extrusion cycles.

Formulation	Size ± SD (nm) Extruded	PdI ± SD
Lipoid S75	76.56 ± 1.93	0.043 ± 0.012
Lipoid S75 + TUDCA	76.03 ± 2.08	0.036 ± 0.010

Table 4
Characteristics of glibenclamide-loaded liposomes.

Formulation	Size ± SD (nm)	PdI ± SD	Zeta Potential (mV)	pH	GLI Conc. ± SD (µg/mL)	% Drug Loading	% Entrapment Efficiency	Flexibility ± SD (mg/s)
Lipoid S75	143.50 ± 14.66	0.197 ± 0.068	−32.50 ± 5.62	7.41 ± 0.01	113.24 ± 37.89	1.49 ± 0.49	50.33 ± 16.84	0.011 ± 0.005
Lipoid S75 + TUDCA	129.93 ± 13.49	0.154 ± 0.040	−40.73 ± 5.61	7.38 ± 0.01	177.30 ± 7.60	2.31 ± 0.10	78.80 ± 3.38	0.848 ± 0.183

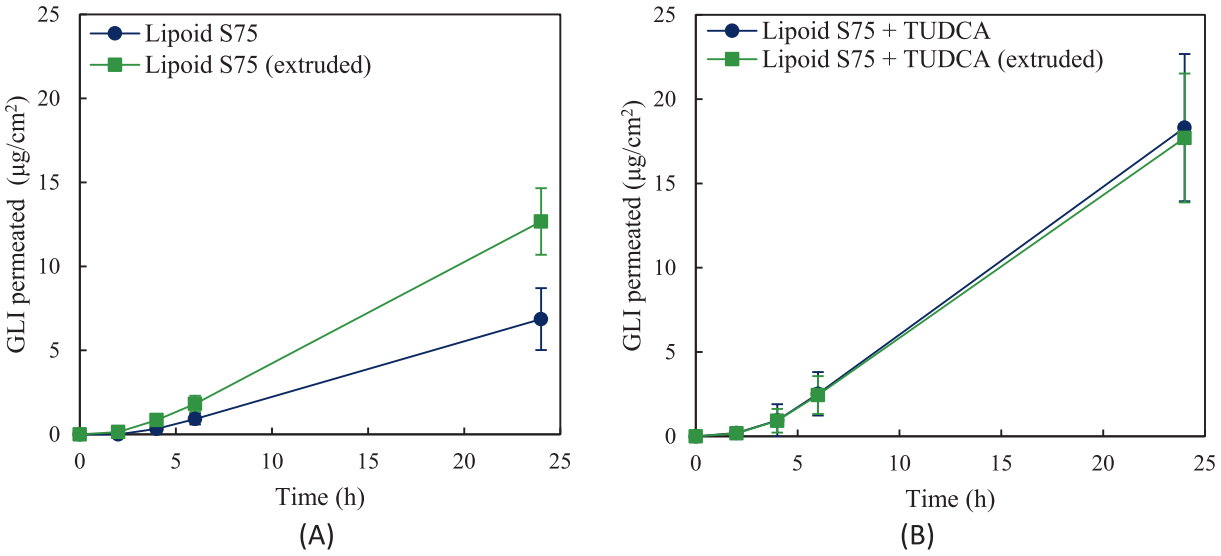


Fig. 5. Permeation of glibenclamide across the sclera (average ± SD) from liposomes extruded and non-extruded made of Lipoid S75 only (Panel A) and made of Lipoid S75 and TUDCA (Panel B).

their shape while diffusing through the tissue, allowing them to reach greater depths before eventually becoming trapped or undergoing partial disruption. Although both extruded and non-extruded TUDCA liposomes possess the same membrane composition and therefore comparable intrinsic flexibility, deformability is expected to play a greater role for the larger vesicles. While extruded liposomes (~76 nm) are already sufficiently small to diffuse through part of the available aqueous pathways, larger liposomes (~130 nm) would require a greater degree of shape adaptation to diffuse through the same porous network.

When comparing liposomes with and without TUDCA, small differences were observed that can be attributed to the different loading of the formulations.

To evaluate the possibility for the sclera to act as a drug reservoir, permeation was monitored after donor removal. Only not-extruded liposomes were evaluated. The donor chamber was filled with the liposomal formulation; after 6 h, the formulation was carefully removed, and glibenclamide permeation was continuously monitored up to 48 h. The collected data (Fig. 6, panel A) showed that initially, even after donor removal, drug permeation continued at a comparable rate, later slowing down and eventually reaching a plateau after approximately 26 h. The amount of drug accumulated in the sclera during the first 6 h represented a high percentage (approx. 80 %) relative to the total, suggesting that liposome-associated drug accumulation in the tissue may promote sustained release and prolonged therapeutic effect. TUDCA liposomes accumulate more drug in the tissue with respect to the conventional formulation, partially due to the higher loading, as can be seen from panel B of Fig. 6.

3.4.3. *Cornea*

The results highlight a significant difference between the two formulations, both in terms of permeation and retention. Glibenclamide encapsulated within conventional liposomes did not permeate through the cornea while liposomes formulated with TUDCA enabled the permeation of glibenclamide after 5 h although in small and variable amounts (1.47 ± 0.42 µg/cm^2), and accumulated 6-fold more drug in the tissue (3.66 ± 0.45 µg/cm^2 or 30 ± 0.01 µg/g) with respect to Lipoid S75 only vesicles (0.57 ± 0.04 µg/cm^2 or 5 ± 0.01 µg/g).

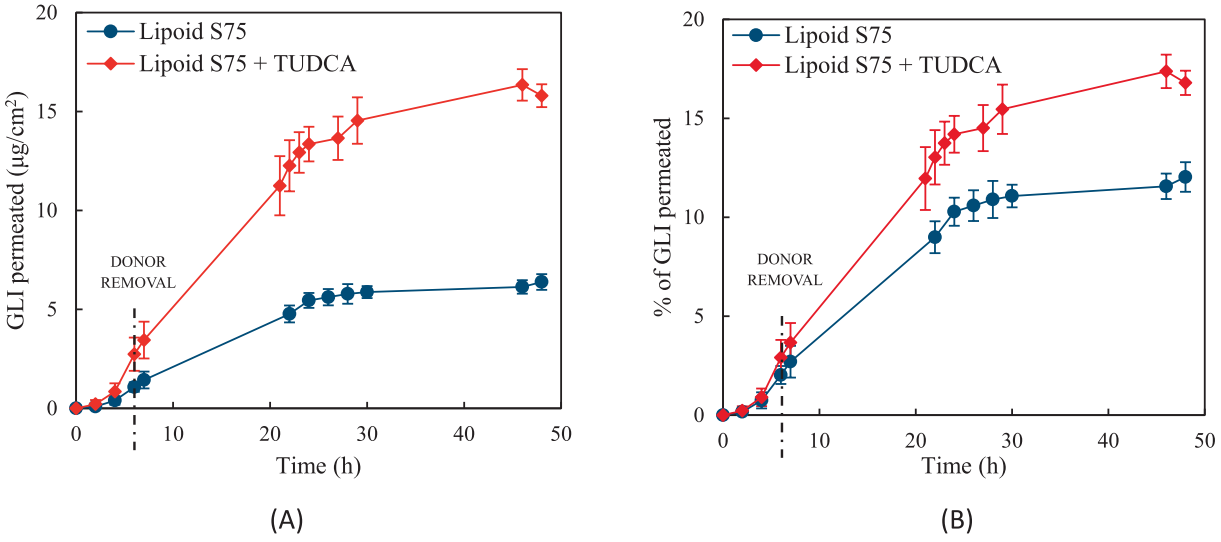


Fig. 6. Permeation of glibenclamide across the sclera (average ± SD) following a 6-hour application of non-extruded liposomes; results are expressed as amount permeated (Panel A) and as a % of applied dose (Panel B) to take into account the different loading.

3.5. Fluorescent probe loading and two-photon microscopy

Different types of fluorescent probes were loaded into liposomes. The deformability test was performed on the formulations loaded with 5 x 10^{-5} M and 10^{-6} M Nile Red (NR), 2 x 10^{-6} M DPH, and 10^{-6} M and 10^{-7} M DiD. The concentrations were selected to obtain a clearly detectable fluorescence signal while avoiding significant alterations to the carrier properties. All loaded probes showed a decrease in the extrusion rate for both normal and TUDCA-modified liposomes (Fig. 7), indicating an increase in the rigidity of the bilayer. In addition, the tests carried out on liposomes with Nile Red and DPH did not show a difference from the respective controls. The difference was instead retained in the case of DiD, which was then used for two-photon microscopy studies.

After application to the sclera for 1 h, images of the sample were acquired. Fig. 8 reports the images of the sclera upon excitation at 1150 nm after the application of liposomes without or with TUDCA, respectively. The green signal coming from Second Harmonic Generation (SHG) is generated by the collagen fibers, while the red signal corresponds to DiD fluorescence (Teng et al., 2006). A porcine scleral sample treated with blank liposomes was used as a control, whose images are reported in the Supplementary Materials (Fig. 3S). In spite of the substantial variability of the tissue, images acquired revealed that the red signal of DiD is more diffuse in TUDCA samples, and reaches a higher penetration depth compared with conventional liposomes (top panels of Fig. 8). We can expect that liposomes of about 140 nm in size will be able to diffuse intact in the relatively big porosity of the scleral tissue, maintaining the lipophilic fluorescent probe embedded within their phospholipid bilayer.

In contrast, liposomes were apparently unable to diffuse intact across the conjunctival and corneal tissues (application time: 2 h). Indeed, as shown in Fig. 9, the red fluorescence signal was confined to the epithelial surface, forming a continuous superficial layer with no detectable signal in the underlying tissue. In this case, the fluorescent probe likely interacts strongly with the plasma membranes. This behavior is typical of dialkylcarbocyanine dyes such as DiD, which bear two long alkyl chains (Fig. 7), insert stably into phospholipid bilayers, and exhibit minimal aqueous solubility and negligible transmembrane permeability (Thermo Fisher Scientific, 2010). Given the markedly different physicochemical properties of the drug (glibenclamide) and the fluorescent probe, their fate across the conjunctiva differs substantially, as indicated by drug transconjunctival permeation profiles (Fig. 4). Although the behavior of the fluorescent probe does not directly reproduce that of the drug itself, the use of DiD remains informative, giving indirect evidence of liposome disruption at the epithelial interface. The distribution of DiD provides strong evidence that a significant fraction of liposomes undergoes destabilization at the epithelial interface. However, the nature of the encapsulated payload may influence the interaction of liposomes with the tissue and their resulting behaviour. It is also worth mentioning that recent FRET-based studies performed with liposomes of different size, composition and surface charge consistently demonstrated the presence of a fraction of intact liposomes (10–50 %) within ocular tissues for at least 60 min (Zhu et al., 2025) suggesting that liposome destabilization upon contact with ocular tissues is a progressive rather than an all-or-none process. Accordingly, it is conceivable that both intact and partially destabilized glibenclamide-loaded liposomes contribute to drug delivery, with membrane deformability favouring their interaction with the epithelial surface, as previously demonstrated for other biological barriers (Schlich et al., 2022).

Further images are shown in the Supplementary Materials.

3.6. Biocompatibility

Bile salts are amphipathic molecules that, due to their detergent properties, are known to exert cytotoxic and irritant effects on cells. However, this characteristic is strictly dependent on the specific chemical structure of each bile salt, with more hydrophilic compounds generally displaying lower toxicity. In general, TUDCA is considered well-tolerated and safe. It has been widely described as an effective hepatoprotective agent and a modulator of endoplasmic reticulum stress (Afşar et al., 2020). Consequently, it has been explored in several therapeutic contexts (Kusaczuk, 2019). With regards to ocular delivery, other negatively charged bile salts have been considered for the formulation of liposomes, showing in general a safe profile in spontaneously derived human corneal epithelial cells, except for sodium deoxycholate (Qi et al., 2013). Given the limited amount of data available on ocular cells, a preliminary study was conducted with TUDCA on the ARPE-19 cell line. Cells were treated with concentrations ranging from 0.5 to 3 mM, and, as shown in Fig. 10, TUDCA maintained approximately 60 % of cell viability across this range, despite the relatively high concentrations tested.

After confirming the tolerability of TUDCA, blank liposomes with/without TUDCA were evaluated. Data obtained demonstrated the cytocompatibility of both types of liposomes and highlighted that the inclusion of TUDCA in the lipidic vesicles further increases its

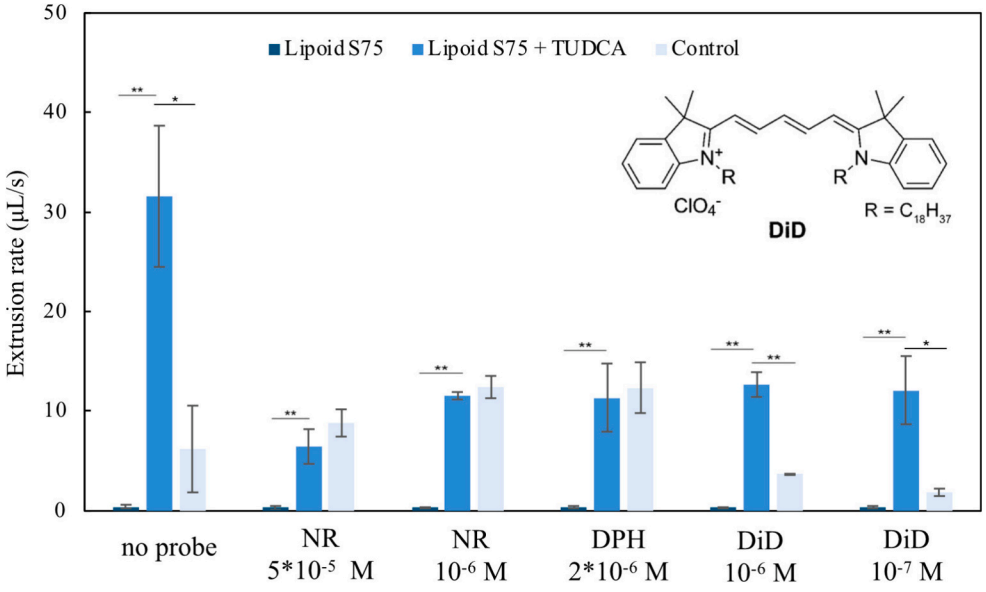


Fig. 7. Extrusion rate of liposomes loaded with fluorescent probes.

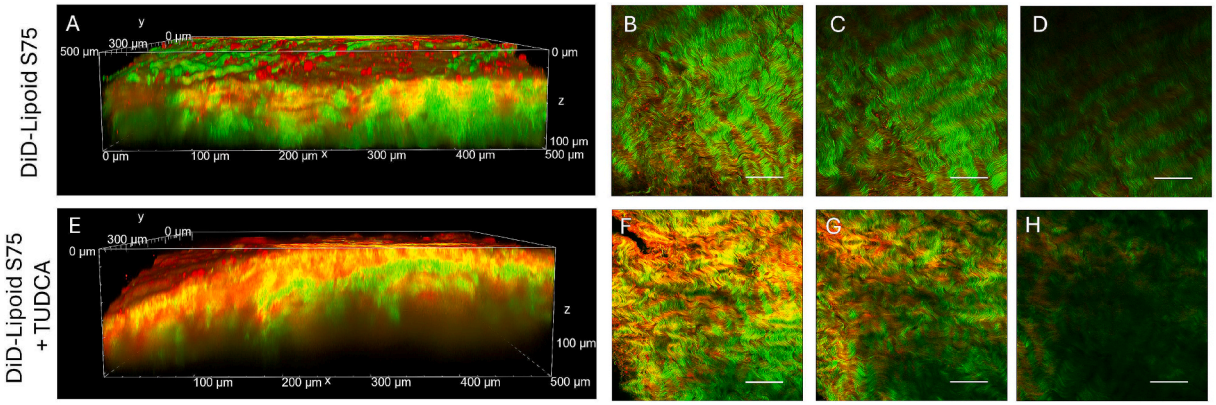


Fig. 8. Z-stack of scleral tissue treated for 1 h with DiD-loaded liposomes (A-E), surface (B-F), depth of 20 μm (C-G), depth of 50 μm (D-H). Scale bar: 100 μm.

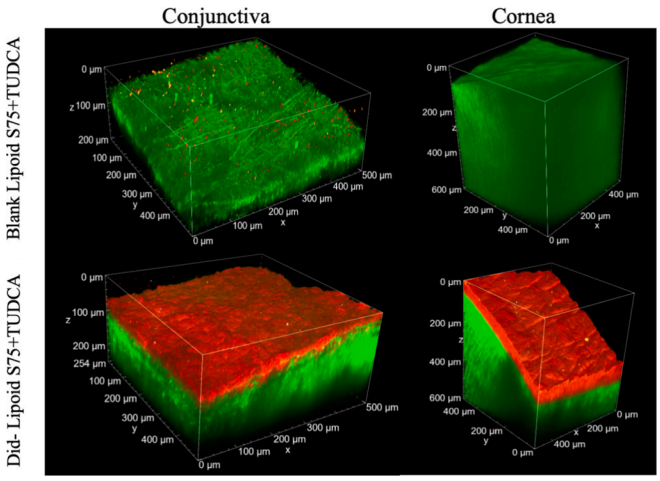


Fig. 9. Z-stack of isolated ocular tissues treated with TUDCA-liposomes (unloaded or loaded with DiD) for 2 h. The top panels show the tissue permeated with blank liposomes (without DiD). At this excitation wavelength, the autofluorescence of epithelium and the SHG of collagene fall in the same channel (green), making them hardly distinguishable. In Supplementary Materials, images of cornea and conjunctiva collected by exciting at 820 nm are shown for comparison (Fig. 4S).

biocompatibility: at 3 mM concentration, the viability increases from 67 to 88 %. This result is in accordance with previous reports showing, in non-ocular models, that the inclusion of bile salts into phospholipids attenuates their toxicity (Tan et al., 2013; Dial et al., 2008).

The cytotoxicity results of GLI-loaded TUDCA-modified liposomes (Panel C) indicate a slight increase in toxicity at concentrations above 25 μg/mL (*approx* 50 μM), in reasonable agreement with data reported in the literature for other cell lines (Wang et al., 2026). Notably, the neuroprotective efficacy of glibenclamide in the retina occurs at much lower concentrations (i.e. 1 nM (Berdugo et al., 2021), indicating that the concentrations used in this study are appropriate and compatible with a favorable safety profile.

3.7. *Freeze-drying*

Liposomes were stored at 4 °C, and the stability after 30 days was evaluated. Data obtained highlight the decrease in the loading of vesicles to around 50 % for all formulations prepared. Liposomes were then freeze-dried in the presence of different cryoprotectants, whose type and concentrations were selected based on a thorough review addressing the critical issues in liposome lyophilization (Franzé et al., 2018). At first, the screening was performed on Lipoid S75-only liposomes, adding the cryoprotectant after vesicles' formation. The size and loading of reconstituted liposomes are listed in Table 6. Before lyophilization, the presence of the protectants did not modify the size and the homogeneity of the vesicles. After reconstitution, only liposomes with lactose as a protectant had dimensions similar to the original form, but the PdI increased markedly. The addition of lactose in the water phase during liposome formation marketly reduced the PDI and preliminary data on GLI encapsulation showed a percentage higher than 90 %. Further studies will be necessary to assess the stability after longer storage time.

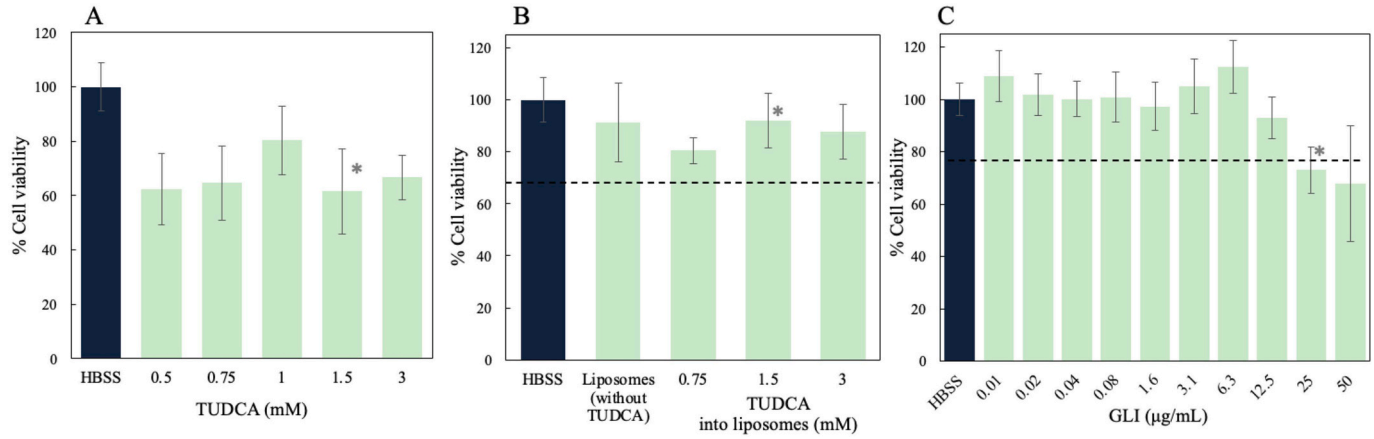


Fig. 10. MTT assay on ARPE-19 cell line treated for 4 h with TUDCA solution (Panel A); blank liposomes with/without TUDCA (Panel B); GLI-loaded TUDCA-modified liposomes (Panel C). In Panel B, liposomes without TUDCA were not diluted. * denotes samples with the same concentration of TUDCA.

Table 6
Size and PDI of liposomes before and after the freeze-drying process with different cryoprotectants. % GLI-retained after the reconstitution of vesicles.

		Before Freeze Drying		After Freeze Drying		
Formulation	**Cryoprotectant (w/w %)**	Size ± SD (nm)	PdI ± SD	Size ± SD (nm)	PdI ± SD	% GLI-retained
Lipoid S75	Glucose7.5 % w/w out[a])	126.0 ± 1.9	0.123 ± 0.011	286.0 ± 72.4	0.666 ± 0.100	80
Lipoid S75	Mannitol (7.5 % w/w out[a])	123.3 ± 1.1	0.145 ± 0.006	484.2 ± 6.4	0.461 ± 0.006	86
Lipoid S75	Sucrose (15 % w/w out[a])	124.3 ± 2.0	0.143 ± 0.006	453.5 ± 12.7	0.462 ± 0.038	67
Lipoid S75	Lactose (15 % w/w out[a])	127.4 ± 0.6	0.145 ± 0.022	149.8 ± 3.2	0.369 ± 0.006	65
Lipoid S75 + TUDCA	Lactose (15 % w/w out[a])	118.9 ± 0.5	0.150 ± 0.006	137.0 ± 0.5	0.448 ± 0.025	83
Lipoid S75	Lactose (5 % w/w in[b], 15 % out[a])	130.8 ± 1.4	0.172 ± 0.006	129.9 ± 0.7	0.223 ± 0.007	90
Lipoid S75 + TUDCA	Lactose (5 % w/w in[b], 15 % out[a])	115.3 ± 1.0	0.140 ± 0.009	125.8 ± 0.4	0.265 ± 0.005	92

[a] Out: cryoprotectant added to the final formulation
[b] In: cryoprotectant added in the aqueous phase before the injection of lipidic phase.

4. Conclusion

Liposomal formulations have been demonstrated to be capable of solubilizing glibenclamide, enabling its possible application at the ocular level in the form of eye drops. The presence of phospholipids may be beneficial for the health of the ocular surface, while the addition of TUDCA may contribute to enhancing the neuroprotective action of the drug. The introduction of TUDCA increased liposome flexibility by inducing a looser and less ordered lamellar architecture, characterized by an increase in interlamellar spacing and a reduction in the number of coherently stacked layers. These nanoscale rearrangements are consistent with a softer and more compliant membrane, in line with enhanced deformability. This has impacted the ability of glibenclamide to accumulate and permeate tissues, also demonstrating an improved reservoir effect in the sclera, potentially capable of prolonging and sustaining drug release over time. The concentrations of glibenclamide loaded into the systems and subsequently released into the tissues appear sufficient to exert biological activity. Indeed, the study by Berdugo et al. (2021) showed that glibenclamide is effective at very low concentrations, with a single intravitreal injection of 0.001 ng/eye being sufficient to induce a significant improvement in retinal function. This raises the possibility that a therapeutically relevant amount could reach the retina. Overall, these results highlight the promising potential of the developed formulation for glibenclamide delivery, also considering the excellent tolerability observed in RPE cells. Although the ex vivo models provide valuable information on the influence of formulation variables on tissue penetration, they cannot fully reproduce the dynamic physiological environment of the eye. Therefore, the ability of topically administered glibenclamide liposomes to achieve therapeutically relevant retinal concentrations remains to be confirmed by appropriate in vivo studies. Stability remains a critical aspect, as lyophilization, although feasible, is associated with complexity and cost. However, from an industrial perspective, the preparation method is scalable and the formulation is compatible with sterilization by filtration, supporting its potential for further development.

CRediT authorship contribution statement

Sofia Dalla Lana: Writing – review & editing, Writing – original draft, Validation, Methodology, Investigation, Conceptualization. **Francesco Bertocchi:** Writing – review & editing, Writing – original draft, Methodology, Investigation. **Caterina Ricci:** Writing – review & editing, Methodology, Investigation, Conceptualization. **Cristina Sissa:** Writing – review & editing, Writing – original draft, Methodology, Funding acquisition, Conceptualization. **Annalisa Bianchera:** Writing – review & editing, Methodology. **Elena Del Favero:** Writing – review & editing, Methodology, Funding acquisition. **Cristina Padula:** Writing – review & editing, Validation, Methodology. **Silvia Pescina:** Writing – review & editing, Validation, Methodology. **Patrizia Santi:** Writing – review & editing, Funding acquisition. **Sara Nicoli:** Writing – review & editing, Writing – original draft, Methodology, Funding acquisition, Conceptualization.

Declaration of competing interest

The authors declare that they have no known competing financial interests or personal relationships that could have appeared to influence the work reported in this paper.

Sara Nicoli is an Associate Editor for *International Journal of Pharmaceutics* and was not involved in the editorial review or the decision to publish this article.

Acknowledgements

The authors thank Ferdinando Ruocco and Macello Annoni SpA for kindly providing procine eye bulbs.

Declaration of generative AI and AI-assisted technologies in the writing process

During the preparation of this work the authors used ChatGPT (OpenAI, GTP-5.5) for the purpose of improving the clarity and accuracy of the English language. After using this tool, the authors reviewed and verified the content as needed and take full responsibility for the content of the publication.

Funding statement

This work has been carried out in the frame of ALIFAR project, funded by Italian Ministry of University and Research through the program 'Dipartimento di Eccellenza 2023-2027'.

SDL benefited of a PhD fellowship financed by the project VISIO (Vesicles investigation through advanced spectroscopic and microscopic techniques for ocular delivery) P2022ALSMP. PNRR Mission 4 "Istruzione e Ricerca" – Component C2. Investment 1.1, "Fondo per il programma Nazionale di Ricerca e Progetti di Rilevante Interesse Nazionale (PRIN).

Appendix A. Supplementary data

Supplementary data to this article, that includes experimental details, methods, tables and figures, can be found online at https://doi.org/10.1016/j.ijpharm.2026.127203.

Data availability

Data will be made available on request.

References

Afşar, E., Kırımlıoglu, E., Çeker, T., Yılmaz, Ç., Demir, N., Aslan, M., 2020. Effect of ER stress on sphingolipid levels and apoptotic pathways in retinal pigment epithelial cells. Redox Biol. 30, 101430. https://doi.org/10.1016/j.redox.2020.101430.

Appell, M.B., Pejavar, J., Pasupathy, A., Rompicharla, S.V.K., Abbasi, S., Malmberg, K., et al., 2024. Next generation therapeutics for retinal neurodegenerative diseases. J. Control. Release 367, 708–736. https://doi.org/10.1016/j.jconrel.2024.01.063.

Badran, M., Shalaby, K., Al-Omrani, A., 2012. Influence of the flexible liposomes on the skin deposition of a hydrophilic model drug, carboxyfluorescein: dependency on their composition. Sci. World J. 12 (2012), 134876. https://doi.org/10.1100/2012/134876. PubMed PMID: 22536120; PubMed Central PMCID: PMC3334324.

Berdugo, M., Delaunay, K., Naud, M.C., Guegan, J., Moulin, A., Savoldelli, M., et al., 2021. The antidiabetic drug glibenclamide exerts direct retinal neuroprotection. Transl. Res. 229, 83–99. https://doi.org/10.1016/j.trsl.2020.10.003.

Chong, D.D., Das, N., Singh, R.P., 2024. Diabetic retinopathy: screening, prevention, and treatment. Cleve. Clin. J. Med. 91 (8), 503–510. https://doi.org/10.3949/ccjm.91a.24028.

Daruich, A., Picard, E., Boatright, J.H., Behar-Cohen, F., 2019. Review: the bile acids urso- and tauroursodeoxycholic acid as neuroprotective therapies in retinal disease. Mol. Vis. 25, 610–624. https://pmc.ncbi.nlm.nih.gov/articles/PMC6817734/.

Daruich, A., Picard, E., Guégan, J., Jaworski, T., Parenti, L., Delaunay, K., et al., 2022. Comparative analysis of urso- and tauroursodeoxycholic acid neuroprotective effects on retinal degeneration models. Pharmaceuticals 15 (3), 334. https://doi.org/10.3390/ph15030334.

Del Favero, E., Pasina, M., Ricci, C., 2024. Polymeric micelles for the delivery of neuroprotective drugs to the retina. https://doi.org/10.15151/ESRF-ES-1975973657.

IDF Diabetes Atlas, 2025. Global Diabetes Data & Insights [Internet]. [cited 2025 Sep 26]. Available from: https://diabetesatlas.org/resources/idf-diabetes-atlas-2025/.

Dial, E.J., Rooijakkers, S.H.M., Darling, R.L., Romero, J.J., Lichtenberger, L.M., 2008. Role of phosphatidylcholine saturation in preventing bile salt toxicity to gastrointestinal epithelia and membranes. J. Gastroenterol. Hepatol. 23 (3), 430–436. https://doi.org/10.1111/j.1440-1746.2007.05153.x.

Franzé, S., Selmin, F., Samaritani, E., Minghetti, P., Cilurzo, F., 2018. Lyophilization of liposomal formulations: still necessary, still challenging. Pharmaceutics 10 (3), 139. https://doi.org/10.3390/pharmaceutics10030139.

Fu, J., Aung, M.H., Prunty, M.C., Hanif, A.M., Hutson, L.M., Boatright, J.H., et al., 2021. Tauroursodeoxycholic acid protects retinal and visual function in a mouse model of type 1 diabetes. Pharmaceutics 13 (8), 1154. https://doi.org/10.3390/pharmaceutics13081154.

Gabai, A., Zeppieri, M., Finocchio, L., Salati, C., 2023. Innovative strategies for drug delivery to the ocular posterior segment. Pharmaceutics 15 (7), 1862. https://doi.org/10.3390/pharmaceutics15071862.

González-Rodríguez, M.L., Arroyo, C.M., Cózar-Bernal, M.J., González-R, P.L., León, J. M., Calle, M., et al., 2016. Deformability properties of timolol-loaded transfersomes based on the extrusion mechanism. statistical optimization of the process. Drug Dev. Ind. Pharm. 42 (10), 1683–1694. https://doi.org/10.3109/03639045.2016.1165691.

Guillot, A.J., Martínez-Navarrete, M., Garrigues, T.M., Melero, A., 2023. Skin drug delivery using lipid vesicles: a starting guideline for their development. J. Control. Release 355, 624–654. https://doi.org/10.1016/j.jconrel.2023.02.006.

Jourdan, J.P., Bureau, R., Rochais, C., Dallemagne, P., 2020. Drug repositioning: a brief overview. J. Pharm. Pharmacol. 72 (9), 1145–1151. https://doi.org/10.1111/jphp.13273.

Khalaf, K., Tornese, P., Cocco, A., Albanese, A., 2022. Tauroursodeoxycholic acid: a potential therapeutic tool in neurodegenerative diseases. Transl. Neurodegener, 11 (1). doi:10.1186/s40035-022-00307-z.

Kumar, D., Tiwari, S., 2025. Bile salts trigger deformability in liposomal vesicles through edge-activating action. Mol. Pharm. https://doi.org/10.1021/acs.molpharmaceut.5c00129.

Kusaczuk, M., 2019. Tauroursodeoxycholate—bile acid with chaperoning activity: molecular and cellular effects and therapeutic perspectives. Cells 8 (12), 1471. https://doi.org/10.3390/cells8121471.

Li, J., Cheng, T., Tian, Q., Cheng, Y., Zhao, L., Zhang, X., et al., 2019. A more efficient ocular delivery system of triamcinolone acetonide as eye drop to the posterior segment of the eye. Drug Deliv. 26 (1), 188–198. https://doi.org/10.1080/10717544.2019.1571122. PubMed PMID: 30835587.

Li, J., Huang, Z., Jin, Y., Liang, L., Li, Y., Xu, K., et al., 2024. Neuroprotective effect of tauroursodeoxycholic acid (TUDCA) on in vitro and in vivo models of retinal disorders: a systematic Review. Curr. Neuropharmacol. 22 (8), 1374–1390. https://doi.org/10.2174/1570159x21666230907152207.

López-Cano, J.J., González-Cela-Casamayor, M.A., Andrés-Guerrero, V., Herrero-Vanrell, R., Molina-Martínez, I.T., 2021. Liposomes as vehicles for topical ophthalmic drug delivery and ocular surface protection. Expert Opin. Drug Deliv. 18 (7), 819–847. https://doi.org/10.1080/17425247.2021.1872542.

Maharjan, R., Jeong, J., Bhujel, R., Kim, M.S., Han, H.K., Kim, N.A., et al., 2022. Correlation of solubility thermodynamics of glibenclamide with recrystallization and in vitro release profile. Molecules 27 (4), 1392. https://doi.org/10.3390/molecules27041392.

Mosallam, S., Sheta, N.M., Elshafeey, A.H., Abdelbary, A.A., 2021. Fabrication of highly deformable bilosomes for enhancing the topical delivery of terconazole: in vitro characterization, microbiological evaluation, and in vivo skin deposition study. AAPS PharmSciTech 22 (2), 74. https://doi.org/10.1208/s12249-021-01924-z.

Park, S., Kim, H.K., 2023. Development of skin-permeable flexible liposome using ergosterol esters containing unsaturated fatty acids. Chem. Phys. Lipids 250, 105270. https://doi.org/10.1016/j.chemphyslip.2022.105270.

Pescina, S., Santi, P., Ferrari, G., Padula, C., Cavallini, P., Govoni, P., et al., 2012. Ex vivo models to evaluate the role of ocular melanin in trans-scleral drug delivery. Eur. J. Pharm. Sci. 46 (5), 475–483. https://doi.org/10.1016/j.ejps.2012.03.013.

Pescina, S., Grolli Lucca, L., Govoni, P., Padula, C., Del Favero, E., Cantù, L., et al., 2019. Ex vivo conjunctival retention and transconjunctival transport of poorly soluble drugs using polymeric micelles. Pharmaceutics 11 (9), 476. https://doi.org/10.3390/pharmaceutics11090476.

Pescina, S., Sala, M., Scala, M.C., Santi, P., Padula, C., Campiglia, P., et al., 2020. Synthesis and ex vivo trans-corneal permeation of penetratin analogues as ophthalmic carriers: preliminary results. Pharmaceutics 12 (8), 728. https://doi.org/10.3390/pharmaceutics12080728.

Picard, E., Youale, J., Hyman, M.J., Xie, E., Achiedo, S., Kaufmann, G.T., et al., 2024. Glyburide confers neuroprotection against age-related macular degeneration (AMD). Transl. Res. 272, 81–94. https://doi.org/10.1016/j.trsl.2024.05.002.

Qi, J., Dai, Z., Lu, Y., Wu, W., Liu, 2013. Liposomes containing bile salts as novel ocular delivery systems for tacrolimus (FK506): in vitro characterization and improved corneal permeation. Int. J. Nanomed. https://doi.org/10.2147/IJN.S44487.

Qi, Q., Wei, Y., Zhang, X., Guan, J., Mao, S., 2023. Challenges and strategies for ocular posterior diseases therapy via non-invasive advanced drug delivery. J. Control. Release 361, 191–211. https://doi.org/10.1016/j.jconrel.2023.07.055.

Sabat, M.J., Wiśniewska-Becker, A.M., Markiewicz, M., Marzec, K.M., Dybas, J., Furso, J., et al., 2021. Tauroursodeoxycholic acid (TUDCA)—lipid interactions and antioxidant properties of TUDCA studied in model of photoreceptor membranes. Membranes 11 (5), 327. https://doi.org/10.3390/membranes11050327.

Schlich, M., Musazzi, U.M., Campani, V., Biondi, M., Franzé, S., Lai, F., et al., 2022. Design and development of topical liposomal formulations in a regulatory perspective. Drug Deliv. Transl. Res. 12 (8), 1811–1828. https://doi.org/10.1007/s13346-021-01089-z.

Sebaaly, C., Greige-Gerges, H., Stainmesse, S., Fessi, H., Charcosset, C., 2016. Effect of composition, hydrogenation of phospholipids and lyophilization on the characteristics of eugenol-loaded liposomes prepared by ethanol injection method. Food Biosci. 15, 1–10. https://doi.org/10.1016/j.fbio.2016.04.005.

Sharma, R., Majer, F., Peta, V.K., Wang, J., Keaveney, R., Kelleher, D., et al., 2010. Bile acid toxicity structure–activity relationships: correlations between cell viability and lipophilicity in a panel of new and known bile acids using an oesophageal cell line (HET-1A). Bioorg. Med. Chem. 18 (18), 6886–6895. https://doi.org/10.1016/j.bmc.2010.07.030.

Singh, S., Verma, D., MohdA, M., Das, A.K., Dudeja, M., Anwer, M.K., et al., 2017. Development and optimization of ketoconazole loaded nano-transfersomal gel for vaginal delivery using Box-Behnken design: in vitro , ex vivo characterization and antimicrobial evaluatio. J Drug Deliv Sci Technol. 39, 95–103. https://doi.org/10.1016/j.jddst.2017.03.007.

Tan, Y., Qi, J., Lu, Y., Hu, F., Yin, Z., Wu, W., 2013. Lecithin in mixed micelles attenuates the cytotoxicity of bile salts in Caco-2 cells. Toxicol. In Vitro 27 (2), 714–720. https://doi.org/10.1016/j.tiv.2012.11.018.

Teng, S.W., Tan, H.Y., Peng, J.L., Lin, H.H., Kim, K.H., Lo, W., et al., 2006. Multiphoton autofluorescence and second-harmonic generation imaging of the ex vivo porcine eye. Investig. Opthalmol. Vis. Sci. 47 (3), 1216. https://doi.org/10.1167/iovs.04-1520.

Teo, Z.L., Tham, Y.C., Yu, M., Chee, M.L., Rim, T.H., Cheung, N., et al., 2021. Global prevalence of diabetic retinopathy and projection of burden through 2045. Ophthalmology 128 (11), 1580–1591. https://doi.org/10.1016/j.ophtha.2021.04.027.

Thermo Fisher Scientific, 2010. Fluorescent Tracers Derivatives of Cell Morphology and Fluid Flow. In: Molecular Probes Handbook.

Trivedi, R., Umekar, M., Kotagale, N., Bonde, S., Taksande, J., 2021. Design, evaluation and in vivo pharmacokinetic study of a cationic flexible liposomes for enhanced transdermal delivery of pramipexole. J. Drug Deliv. Sci. Technol. 61, 102313. https://doi.org/10.1016/j.jddst.2020.102313.

Varela-Fernández, R., Díaz-Tomé, V., Luaces-Rodríguez, A., Conde-Penedo, A., García-Otero, X., Luzardo-Álvarez, A., et al., 2020. Drug delivery to the posterior segment of the eye: biopharmaceutic and pharmacokinetic considerations. Pharmaceutics 12 (3), 269. https://doi.org/10.3390/pharmaceutics12030269.

Wang, P., Xie, J., Xiang, F., Xiong, S., Li, Y., Xia, B., et al., 2026. Hepato-ocular crosstalk: bile acids bridging pathogenesis and therapy. iScience. 29(3):115118. doi:10.1016/j.isci.2026.115118.

World Health Organization, 2019. World report on vision.

Yang, Y., Lockwood, A., 2022. Topical ocular drug delivery systems: innovations for an unmet need. Exp. Eye Res. 218, 109006. https://doi.org/10.1016/j.exer.2022.109006.

Zhao, J., Mao, S., 2021. Tuning the membrane fluidity of liposomes for desirable in vivo fate with enhanced drug delivery. In: Advances in Biomembranes and Lipid Self-Assembly. Elsevier, pp. 67–106. https://doi.org/10.1016/bs.abl.2021.11.003.

Zhu, X., Li, S., Huang, J., Yin, C., Li, Y., Guo, W., et al., 2025. FRET-based analysis on the fate of liposome and cyclodextrin@liposome nanocomposites from ocular surface to the posterior segment of the eye. J. Control. Release 377, 794–809. https://doi.org/10.1016/j.jconrel.2024.11.079.